Optic atrophy–associated TMEM126A is an assembly factor for the ND4-module of mitochondrial complex I

Luke E. Formosa[a,1], Boris Reljic[a,b], Alice J. Sharpe[a], Daniella H. Hock[b], Linden Muellner-Wong[a,b], David A. Stroud[b], and Michael T. Ryan[a,1]

[a]Department of Biochemistry and Molecular Biology, Monash Biomedicine Discovery Institute, Monash University, VIC, 3800, Melbourne, Australia; and [b]Department of Biochemistry and Pharmacology, The Bio21 Institute, The University of Melbourne, VIC, 3000, Melbourne, Australia

Edited by Jodi Nunnari, University of California, Davis, CA, and approved March 11, 2021 (received for review September 19, 2020)

Mitochondrial disease is a debilitating condition with a diverse genetic etiology. Here, we report that TMEM126A, a protein that is mutated in patients with autosomal-recessive optic atrophy, participates directly in the assembly of mitochondrial complex I. Using a combination of genome editing, interaction studies, and quantitative proteomics, we find that loss of TMEM126A results in an isolated complex I deficiency and that TMEM126A interacts with a number of complex I subunits and assembly factors. Pulse-labeling interaction studies reveal that TMEM126A associates with the newly synthesized mitochondrial DNA (mtDNA)-encoded ND4 subunit of complex I. Our findings indicate that TMEM126A is involved in the assembly of the ND4 distal membrane module of complex I. In addition, we find that the function of TMEM126A is distinct from its paralogue TMEM126B, which acts in assembly of the ND2-module of complex I.

mitochondria | complex I | oxidative phosphorylation | optic atrophy | membrane protein

Mitochondria are hubs of metabolic and biosynthetic activity and also play important roles in a variety of cellular processes that include antiviral signaling, calcium handling, and cell death (1). Mutations in at least 289 genes that encode mitochondrial proteins have a negative effect on mitochondrial homeostasis and are associated with mitochondrial disease (2). A large proportion of these mitochondrial proteins have a direct role in energy conversion as they are required as structural subunits or assembly factors for the oxidative phosphorylation (OXPHOS) system (3). Additional gene products that are mutated in mitochondrial disease have various roles including the maintenance and expression of mitochondrial DNA (mtDNA), assembly of iron–sulfur clusters, lipid metabolism, mitochondrial dynamics, and protein import/processing that are secondary to energy conversion processes (4). However, in many cases, it is unclear what the molecular role of some mitochondrial disease–associated genes are, making clinical interventions difficult.

One such example is the role of TMEM126A in mitochondrial function. A homozygous nonsense mutation in the gene encoding TMEM126A (p. Arg55X) was first identified in individuals with autosomal-recessive optic atrophy (AROA) (5). Since then, other patients with AROA have been identified with the same mutation in the *TMEM126A* gene (6, 7). The proximal geography of the individuals identified (Morocco and Tunisia), together with similarities in microsatellite analysis at that locus suggest a founder effect may be responsible for this mutation (5). More recently, individuals with additional novel missense mutations in *TMEM126A* have been identified with AROA (8, 9). Patients identified with mutations in *TMEM126A* generally present with bilateral deficiency in visual acuity with onset from infancy to 6 y of age, optic nerve pallor, and central scotoma (5). Retinal ganglion cells are particularly susceptible to mitochondrial dysfunction as the intraocular length of the axons that form the optic nerve remain unmyelinated and so are highly dependent on adenosine triphosphate (ATP) to propagate the action potential to the visual cortex (10). In addition to AROA, some patients also presented with moderate hypertrophic cardiomyopathy and mild hearing loss (5).

TMEM126A has been reported to be a mitochondrial inner membrane protein that is enriched in the cristae (11); however, its molecular function is unclear. While TMEM126A is metazoan specific, its paralog TMEM126B is found in mammals following a gene duplication event (12). TMEM126B is essential for the biogenesis of respiratory chain complex I as a membrane-integrated assembly factor and central component of the mitochondrial complex I intermediate assembly (MCIA) complex (13–15). Complex I is assembled via the integration of 45 subunits into a number of intermediate modules and at least 15 assembly factors that come together in the mitochondrial inner membrane (16–21). The MCIA complex is involved in assembly of the ND2 membrane module (14, 17). While it has been suggested that TMEM126A may play a compensatory role in patient cells with mutations in TMEM126B (22), the clinical presentation of the two markedly differ (AROA versus late-onset myopathy) (23). Nevertheless, a role for TMEM126A in complex I assembly may be implicated given that it was found enriched with the complex I assembly factors DMAC1 (16), TMEM186, and COA1 (14), as well as with the general mitochondrial insertase OXA1L (24).

Given that mutations in mitochondrially encoded complex I subunits can result in a range of diseases including Leber's Hereditary Optic Neuropathy (LHON) (25, 26), we sought to determine if TMEM126A plays a direct or indirect role in the assembly of mitochondrial OXPHOS complexes, particularly

Significance

Mitochondria are critical organelles that play a central role in energy conversion in cells. Mutations in genes encoding mitochondrial proteins can lead to disease. Here, we discover that the optic atrophy–associated mitochondrial disease gene TMEM126A plays a role in the assembly of the first enzyme of the respiratory chain, complex I. Critically, we show that TMEM126A interacts in a complex with newly synthesized ND4, a highly hydrophobic subunit of complex I that is encoded by mitochondrial DNA. Our findings expand the molecular machinery required to build complex I from its constituent subunits and elucidates the function of a gene mutated in mitochondrial disease.

Author contributions: L.E.F., D.A.S., and M.T.R. designed research; L.E.F., B.R., A.J.S., D.H.H., and L.M.-W. performed research; L.E.F., B.R., A.J.S., D.H.H., L.M.-W., D.A.S., and M.T.R. analyzed data; and L.E.F. and M.T.R. wrote the paper.

The authors declare no competing interest.

This article is a PNAS Direct Submission.

[1]To whom correspondence may be addressed. Email: Luke.Formosa@monash.edu or Michael.Ryan@monash.edu.

This article contains supporting information online at https://www.pnas.org/lookup/suppl/doi:10.1073/pnas.2019665118/-/DCSupplemental.

Published April 20, 2021.

complex I. Complete loss of TMEM126A results in isolated complex I deficiency, with decreased levels of the fully assembled enzyme as well individual complex I subunits. Furthermore, we show that TMEM126A interacts with complex I subunits and assembly factors under steady-state conditions and enriches with the newly translated mitochondrially encoded ND4 subunit. Importantly, we establish that TMEM126A does not play a compensatory role to TMEM126B but rather highlight that it functions in the biogenesis of a distinct assembly module of complex I.

Results

Complex I Deficiency in TMEM126A Knockout Cells. In order to investigate the role of TMEM126A in mitochondrial function, we generated knockout (T126A^{KO}) cell lines using genome editing. Sodium dodecyl-sulfate polyacrylamide gel electrophoresis (SDS-PAGE) and subsequent Western blot analysis of isolated mitochondria revealed the absence of TMEM126A from T126A^{KO} cells (Fig. 1*A*). Sequencing of alleles also confirmed the presence of indels that disrupt the open reading frame (*SI Appendix*, Table S1). Next, to determine how the loss of TMEM126A affected the mitochondrial proteome, unbiased stable isotope labeling by/with amino acids in cell culture (SILAC) quantitative proteomics analysis was performed (Fig. 1*B* and Dataset S1). Complex I subunits were clearly reduced in the T126A^{KO} mitochondria relative to the controls (Fig. 1*B* and Dataset S1). Using the proteomic data from T126A^{KO} cells, a topographical proteomic heatmap was fitted onto the molecular structure of human complex I (27). Subunits belonging to distinct assembly modules of complex I—namely the *N*-, Q-, ND2-, and ND4-modules—were significantly reduced relative to control mitochondria (Fig. 1*C*).

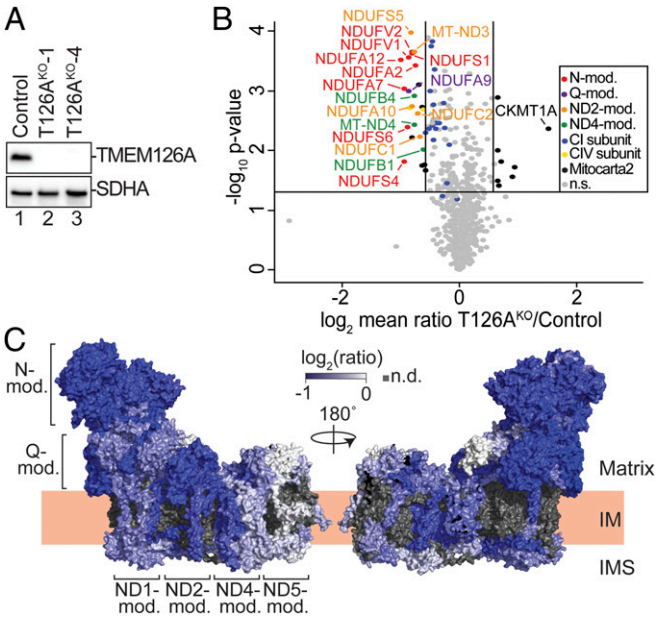

Fig. 1. Complex I subunits reduced in T126A^{KO} mitochondria. (*A*) Isolated mitochondria from control and T126A^{KO} cell lines were subjected to SDS-PAGE and immunoblot analysis. SDHA was used as a loading control. (*B*) Volcano plot of mitochondrial protein abundance in T126A^{KO} cells relative to control. SILAC ratios were $\log_2$ transformed and the mean ($n = 3$) plotted against -$\log_{10}$(*P* value) from single-sample, two-sided Student's *t* test. The horizontal line indicates $P = 0.05$; the vertical lines indicate 1.5-fold change. The blue dots represent complex I subunits with a fold change less than 1.5. (*C*) Topographical heatmap of subunit ratios were fitted to complex I (PDB: 5XTH) (27). The gray regions represent subunits that were not reliably detected (n.d.).

Loss of these subunits correlate with defects in the biogenesis of the membrane arm of complex I (16). The *N*-module is commonly reduced in all cases where complex I assembly is perturbed (16). In contrast, the most up-regulated protein in T126A^{KO} mitochondria was the U-type Creatine Kinase CKMT1A, an enzyme required for maintaining energy homeostasis and buffering ATP levels in cells (28).

Loss of TMEM126A Leads to an Isolated Complex I Defect. Given the observed decrease in complex I subunits by SILAC proteomics, we isolated mitochondria from control and T126A^{KO} cells and assessed complex I assembly by blue native-PAGE (BN-PAGE) and Western blotting (Fig. 2*A*). Solubilization of mitochondrial membranes in the mild detergent digitonin maintains complex I in its supercomplex form with complexes III and IV, while the harsher detergent Triton X-100 dissociates the supercomplex into the holo-complex forms (29). Immunoblotting for the complex I subunit NDUFB8 revealed a reduction in the levels of the supercomplex and in the complex I holoenzyme in comparison to control mitochondria (Fig. 2*A*). Quantification of the NDUFB8 signal showed that the supercomplex was reduced by ~50% of control levels, while the levels of holo-complex I were reduced to ~30% to that of control mitochondria (Fig. 2*B*). In addition, a faster-migrating species at ~440 kDa following digitonin solubilization and ~400 kDa following Triton X-100 solubilization was also apparent (indicated by *; Fig. 2*A*). Given that the NDUFB8 subunit is located at the distal end of the complex I membrane arm (30, 31), this subcomplex may represent an accumulation or breakdown product of this region in the absence of proper complex I assembly. In-gel nicotinamide adenine dinucleotide (NADH) dehydrogenase activity showed that the residual complex I observed in T126A^{KO} cells was still active (Fig. 2*C*). Besides the complex I supercomplexes, OXPHOS complexes III, IV, or V were not changed in T126A^{KO} mitochondria (Fig. 2*D*; note levels of holo-complexes III and IV in lanes 4 to 6 and 10 to 12 respectively), consistent with proteomic analysis.

TMEM126A Associates with Complex I Subunits, Assembly Factors, and Newly Synthesized ND4. Next, we complemented the knockout cells with a construct expressing TMEM126A with a C-terminal Flag epitope tag (TMEM126A^{Flag}) and demonstrated rescue of the complex I assembly defect (Fig. 3*A*). We subsequently performed affinity-enrichment (AE) and label-free quantitative (LFQ) mass spectrometry analysis to determine TMEM126A-interacting partners. TMEM126A^{Flag} was able to enrich ND4 and all accessory subunits of the ND4-module (NDUFB1, NDUFB4, NDUFB5, NDUFB10, and NDUFB11) as well some subunits of the Q- (NDUFS2), ND1- (NDUFA8, NDUFA13, and NDUFA3), ND2- (NDUFA10), and ND5- (NDUFB6, NDUFB8, and NDUFB9) modules (Fig. 3*B* and Dataset S2). Furthermore, TMEM126A^{Flag} enriched a number of complex I assembly factors including the MCIA complex factors ECSIT and ACAD9, the ND1-module assembly factor TIMMDC1, plus the Q-module assembly factors NDUFAF3 and NDUFAF4. TMEM70, an assembly factor recently implicated in the assembly of the complex I ND4-module was also enriched (17, 32). In agreement with previous studies (24), we also observed that TMEM126A^{Flag} was able to enrich the general membrane insertase for mtDNA-encoded proteins, OXA1L. Defects in complex I assembly lead to the accumulation of assembly intermediates consisting of assembly factors and complex I modules. Neither the major MCIA complex at ~450 kDa (involved in ND2-module assembly; Fig. 3*C*, ◊) nor the TIMMDC1 complexes at ~400/440 kDa (involved in ND1-module assembly; Fig. 3*C*, §) were altered in T126A^{KO} mitochondria. However, a higher-molecular–weight species of ~720 kDa (containing both MCIA and TIMMDC1; Fig. 3*C*, labeled #) representing an

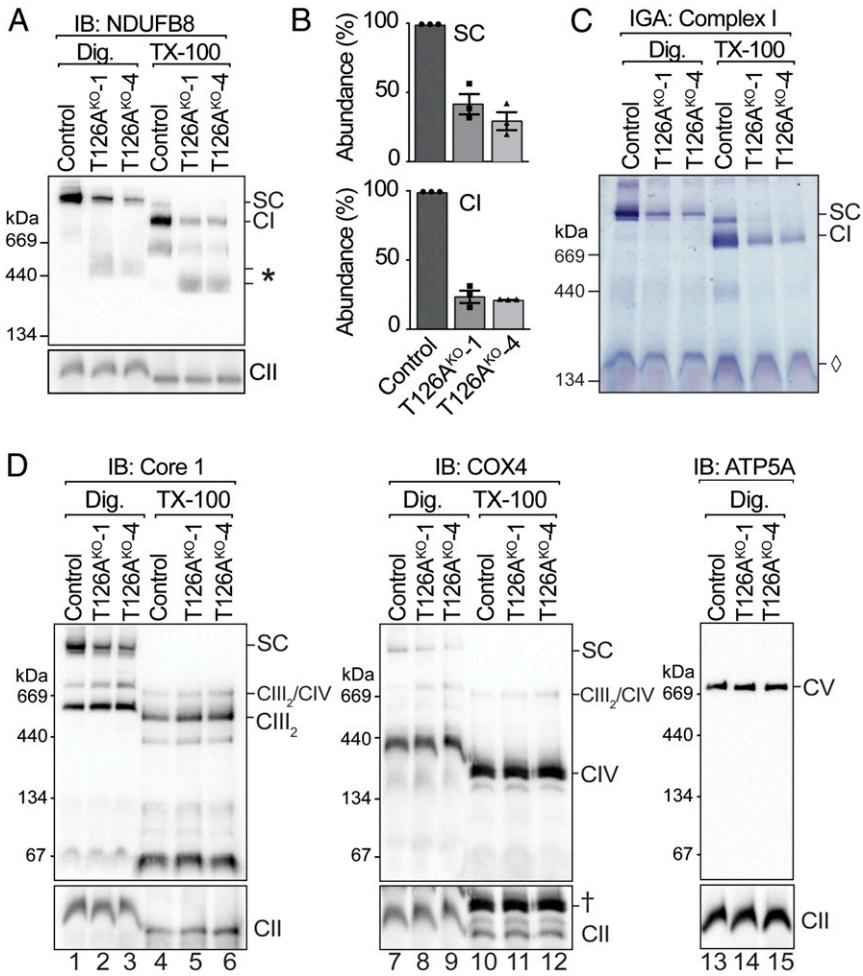

Fig. 2. T126A^{KO} cells have an isolated complex I deficiency. (*A*) Mitochondria were isolated from control and T126A^{KO} cell and subjected to BN-PAGE and Western blotting for complex I (NDUFB8) and complex II (SDHA) used as a control. *, distal membrane arm subcomplex. (*B*) The relative abundance of fully assembled supercomplex and complex I was quantified (mean ± SEM, $n = 3$). (*C*) In-gel complex I activity assay using isolated mitochondria. ◊, Dihydrolipoamide dehydrogenase activity (65). (*D*) Isolated mitochondria subjected to BN-PAGE and Western blotting for complexes III (Core 1), IV (COX4), and V (ATP5A). †, residual COX4 signal following reprobe.

intermediate further along the assembly pathway, was reduced in T126A^{KO} relative to control mitochondria (Fig. 3*C*). These results suggest that while TMEM126A may not participate in complex I assembly directly with the MCIA or TIMMDC1 assembly complexes, loss of TMEM126A impairs later stages of the assembly pathway involving these machineries.

To investigate TMEM126A-containing complexes in more detail, we investigated changes using representative complex I accessory subunit knockout cell lines of each module (16) (Fig. 3*D*). In control cells, TMEM126A mainly migrated as a low-molecular–weight species with a portion of it forming higher-molecular–weight complexes ∼440 kDa to ∼1 MDa in size (Fig. 3*D*). These complexes were the same in NDUFS4^{KO} mitochondria, suggesting that they are independent of the *N*-module. Analysis of NDUFA5^{KO}, NDUFA8^{KO}, NDUFC2^{KO}, and NDUFB7^{KO}, which represent the Q-, ND1, ND2, and ND5-modules, respectively, showed an accumulation of the ∼440 kDa complexes. This suggests that defects in the assembly of the membrane arm of complex I affect TMEM126A-containing complexes. Moreover, the ∼440 kDa complexes were lost in NDUFB10^{KO} mitochondria (representing the ND4-module). Given that all other subunits of the ND4-module are lost in NDUFB10^{KO} (16) this suggests that TMEM126A-containing complexes are dependent on the subunits of the ND4-module for their formation.

Given these results, we assessed whether TMEM126A^{Flag} engages with specific, newly synthesized mtDNA-encoded subunits. We performed pulse labeling of mtDNA-encoded proteins in cells using [^{35}S]-Methionine in the presence of anisomycin (to block cytosolic translation) for 2 h, before removal of the radiolabel and anisomycin for up to 24 h to allow for maturation of the subunits and their assembly into the OXPHOS complexes (33). Following Flag coimmunoprecipitation, samples were subjected to SDS-PAGE and western transfer before phosphorimage analysis. A strong but transient enrichment of TMEM126A^{Flag} with mtDNA-encoded complex I subunit ND4 was observed (Fig. 3*E*). The ND4 subunit was not clearly identified in "total" samples, indicating that the enrichment of this protein by TMEM126A^{Flag} was highly efficient. The identity of the radiolabeled product as ND4 was confirmed by Western blot analysis (*SI Appendix*, Fig. S1). The relatively minor association between TMEM126A^{Flag} with ND1 and ND2 is also consistent with the proteomic analysis and suggests that TMEM126A is involved in assembly of the ND4-module even during integration with the other assembly modules (16). As expected for an assembly factor,

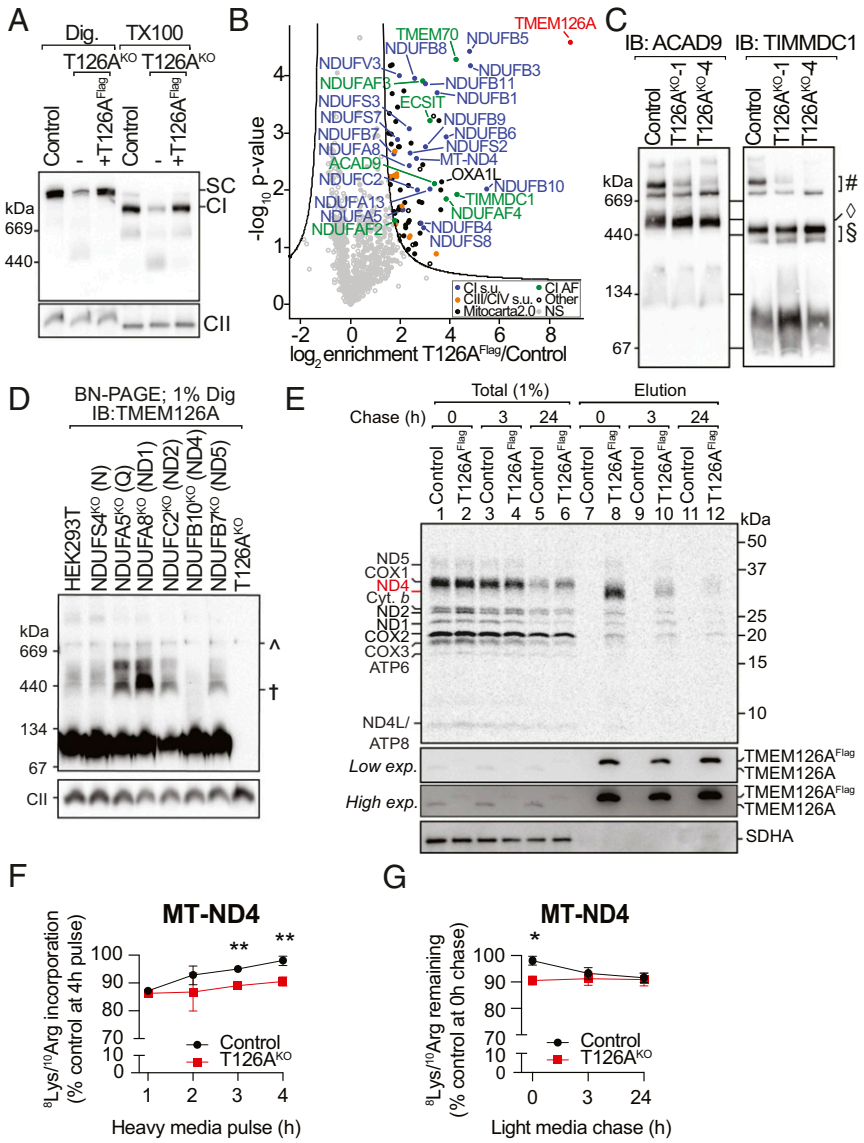

Fig. 3. TMEM126A interacts with the ND4-module during complex I assembly. (*A*) Mitochondria isolated from control, T126A^{KO}-1, and T126A^{KO}-1 +TMEM126A^{Flag} cells and were subjected to BN-PAGE and Western blot analysis. Complex II (SDHA) was used as a loading control. (*B*) Digitonin-solubilized mitochondria from control and T126A^{KO}-1 +TMEM126A^{Flag}–expressing cells were subjected to affinity enrichment using anti-Flag agarose beads. Elutions were subjected to LFQ proteomics. Significance was determined through a two-sided, two-sample *t* test using permutation-based FDR statistics. The curved represents FDR < 1% using an s0 parameter of 1.5. (*C*) Mitochondria from control and T126A^{KO} cells were solubilized in digitonin and analyzed by BN-PAGE and immunoblotting using antibodies as indicated. ◊, ∼450 kDa MCIA complex; §, 400/440 kDa TIMMDC1 complex; #, 720 kDa complex. (*D*) Mitochondria from control and complex I accessory subunit KO cells were isolated and analyzed by BN-PAGE and Western blotting using TMEM126A antibodies. Complex II (SDHA) was used as a loading control. Lower TMEM126A signal is saturated to detect higher-molecular–weight complexes. †, Accumulated TMEM126A complex; ^, nonspecific signal. (*E*) Pulse-labeled mtDNA-encoded subunits from control and T126A^{KO}-1 +TMEM126A^{Flag}–expressing cells were chased for the indicated times, Isolated mitochondria were solubilized in digitonin and subjected to affinity enrichment, SDS-PAGE analysis, and phosphorimaging. Immunoblotting for TMEM126A and SDHA served as controls. (*F*) Pulse SILAC analysis of newly translated MT-ND4 in control and T126A^{KO} cells. Log_2 transformed heavy peptide–derived intensities were plotted relative to control intensities. The data are represented as mean ± SD $n = 3$. (*G*) As for *F* but heavy media exchanged with light media after a 4 h pulse and cells harvested after 3 and 24 h. The data are represented as mean ± SD $n = 3$. *FDR < 0.05 and **FDR < 0.01.

the interaction between TMEM126A and the ND4-module is transient since it is not part of the final assembled complex I.

Given the strong association between TMEM126A and newly translated ND4, we sought to determine whether loss of TMEM126A affected ND4 synthesis and/or stability. Since ND4 radiolabeling was inefficient, we performed a SILAC-based pulse labeling with heavy Lysine (^{8}Lys) and Arginine (^{10}Arg) followed by proteomic analysis (34). Over a 4 h pulse, ND4 incorporated heavy Lys/Arg amino acids more slowly relative to control cells, suggesting that the translation and/or stability of newly synthesized ND4 is disrupted in T126A^{KO} cells (Fig. 3*F* and Dataset S3). Other mtDNA-encoded subunits behaved similarly between control and T126A^{KO} cells (*SI Appendix*, Fig. S2*A* and Dataset S3). To determine if the loss of TMEM126A resulted in changes in subunit stability, samples were labeled for 4 h with heavy amino acids (representing the "0 h chase") and subsequently chased in the presence of light amino acids for 3 and 24 h (Fig. 3*G*). Proteomics analysis showed that the loss of TMEM126A did not

affect the rate of turnover of the majority of detected mtDNA-encoded proteins, including ND4 (Fig. 3*G*, *SI Appendix*, Fig. S2*B*, and Dataset S3). There was some overall reduction in the starting level of ND1; however, the rate of turnover did not increase in the absence of TMEM126A. These results suggest that TMEM126A functions in the early stages of ND4 biogenesis.

TMEM126A Functions Independently of TMEM126B in Complex I Assembly. TMEM126A and its paralog TMEM126B diverged at the root of mammalian evolution; homologs of TMEM126A are present in metazoans while TMEM126B appears confined to mammals (12). We questioned whether the residual assembly of complex I in TMEM126A-deficient cells may be due to the presence of TMEM126B playing a compensatory role. If so, we reasoned that overexpression of TMEM126B in T126A^{KO} cells would enhance complex I assembly. However, additional expression of TMEM126B^{Flag} was not able to rescue complex I levels in T126A^{KO} mitochondria (Fig. 4 *A* and *B* and *SI Appendix*, Fig. S3), suggesting that TMEM126A and TMEM126B do not have overlapping functions. Expression of TMEM126A^{Flag} was able complement this assembly defect as expected (Fig. 4*A* and *SI Appendix*, Fig. S3).

While TMEM126B does not complement the loss of TMEM126A, it has been posed that the reverse may be true. Using proteomic analysis of BN-PAGE gel slices from fibroblasts with pathogenic *TMEM126B* mutations, Sánchez-Caballero and colleagues (22) found that TMEM126A comigrated with the remaining components of the MCIA complex. This led to the conclusion that TMEM126A plays a compensatory role in the absence of TMEM126B (22). Indeed, we also observed an accumulation of a ~400 kDa TMEM126A complex in TMEM126B knockout mitochondria (Fig. 4*C*; †). However, when we assessed mitochondria lacking MCIA core subunits (NDUFAF1^{KO}, ECSIT^{KO}, or ACAD9^{KO} lines), which leads to complete loss of the MCIA complex (14), TMEM126A complexes were still present and accumulated even further (Fig. 4*C*). Thus, TMEM126A-containing complexes are independent of the MCIA and the faster-migrating TMEM126A complex represents an independent species that accumulates due to a disruption in complex I assembly.

Furthermore, we generated a TMEM126A/TMEM126B double-knockout (T126A/B^{DKO}) cell line and found that the stabilities of TMEM126A and TMEM126B are independent of each other (Fig. 4*D* and *SI Appendix*, Table S1). The levels of ND4 and NDUFB10 (an ND4-module subunit) were reduced in T126A^{KO} (Fig. 4*E*). In T126B^{KO}cells and T126A/B^{DKO}, these subunits were even more reduced due to the stronger complex I assembly defect observed (14). Consistent with this, BN-PAGE analysis showed a reduction of ND4 in the supercomplex in T126A^{KO}

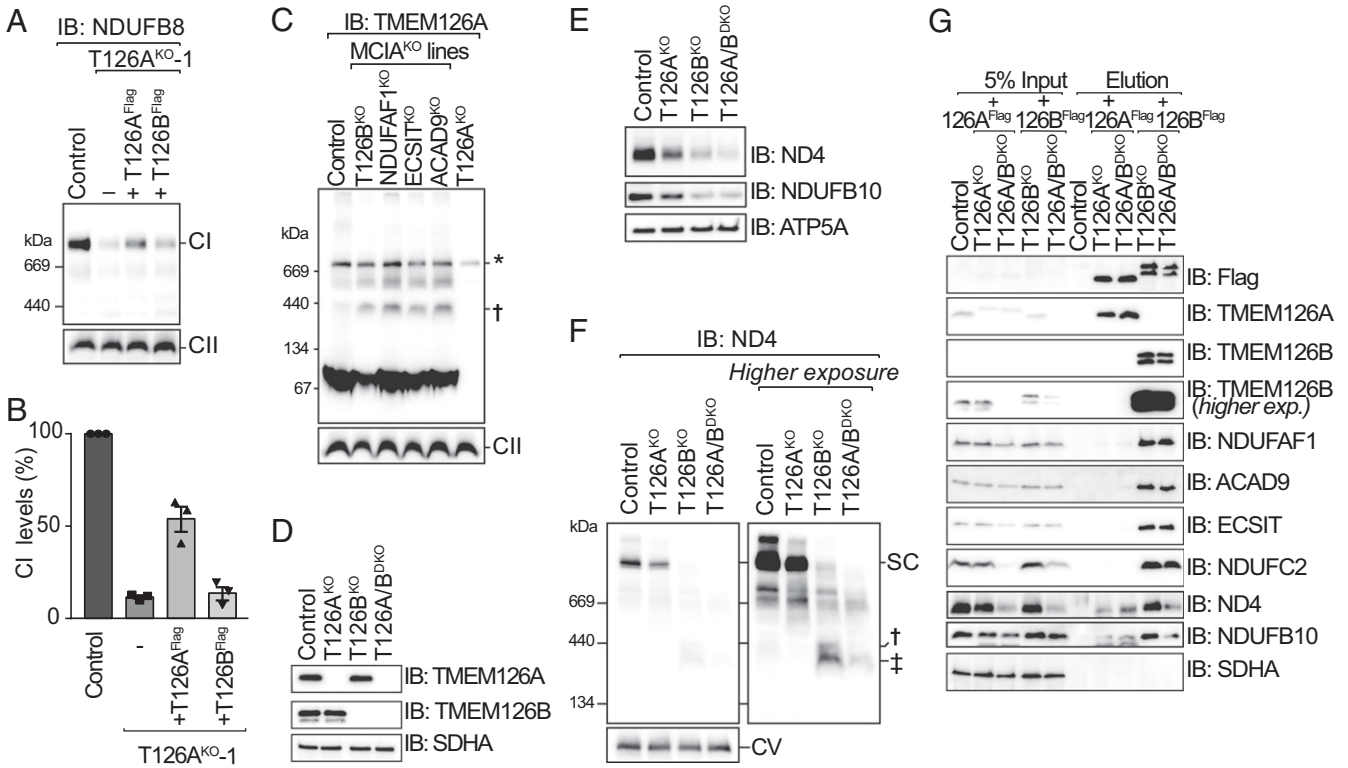

Fig. 4. TMEM126A functions independently of TMEM126B. (*A*) Mitochondria isolated from control, T126A^{KO}-1, and T126A^{KO}-1 expressing TMEM126A^{Flag} or TMEM126B^{Flag} cells were analyzed by BN-PAGE after solubilization in 1% TX100 and immunoblotted for the complex I subunit NDUFB8. SDHA/CII was used as a loading control (*B*) The relative abundance of fully assembled complex I (from *A*) was quantified in control and T126A^{KO} cells expressing TMEM126A^{Flag} and TMEM126B^{Flag} as indicated (mean ± SEM, $n = 3$). (*C*) Mitochondria from MCIA^{KO} and T126A^{KO} cells were analyzed by BN-PAGE following 1% digitonin solubilization and immunoblotting using TMEM126A antibodies. CII (SDHA) was used as a loading control. Lower TMEM126A signal is saturated to detect higher-molecular–weight complexes. †, accumulated TMEM126A complex; *, nonspecific signal. (*D*) Mitochondria were isolated from control, T126A^{KO}, T126B^{KO}, and T126A/B^{DKO} cells and analyzed by SDS-PAGE and Western blotting with antibodies as shown. SDHA was used as a loading control. (*E*) Mitochondria were isolated from control, T126A^{KO}, T126B^{KO}, and T126A/B^{DKO} cells and analyzed by SDS-PAGE and Western blotting with antibodies as shown. ATP5A was used as a loading control. (*F*) Mitochondria from control, T126A^{KO}, T126B^{KO}, and T126A/B^{DKO} cells were analyzed by BN-PAGE following 1% digitonin solubilization and immunoblotting using ND4 antibodies. CV (ATP5A) was used as a loading control. †, accumulated TMEM126A complex; ‡, accumulated ND4-module. (*G*) Mitochondria were isolated from cells expressing TMEM126A^{Flag} or TMEM126B^{Flag} as indicated, solubilized in 1% digitonin, and subjected to Flag affinity enrichment prior to SDS-PAGE analysis. Immunoblotting was performed with antibodies as indicated.

cells, while T126B^{KO} and T126A/B^{DKO} cells did not harbor any fully assembled complex I (Fig. 4*F*). Following loss of TMEM126B, and hence loss of complex I assembly, lower-molecular–weight ND4 assemblies accumulated at ∼400 and ∼350 kDa (Fig. 4*F*; † and ‡). These assemblies were dependent on TMEM126A—with the loss of the ∼400 kDa complex and reduction of the ∼350 kDa complex—indicating that TMEM126A and TMEM126B function at different steps.

Finally, we expressed TMEM126A^{Flag} or TMEM126B^{Flag} in the T126A/B^{DKO} cell line and performed coimmunoprecipitation and SDS-PAGE analysis (Fig. 4*G*). TMEM126B^{Flag} but not TMEM126A^{Flag} efficiently enriched MCIA subunits ACAD9, ECSIT, and NDUFAF1 along with the complex I subunit NDUFC2. No enrichment of MCIA subunits with TMEM126A^{Flag} was seen in the absence of TMEM126B, indicating that TMEM126A does not act as a substitute for TMEM126B. TMEM126A^{Flag} efficiently enriched ND4 and NDUFB10 in the presence or absence of TMEM126B. While TMEM126B also enriched these subunits, the efficiency of enrichment was reduced in the absence of TMEM126A. This is consistent with the role of TMEM126A acting early in the biogenesis of ND4 while TMEM126B (and the MCIA complex) functions at later steps of complex I assembly that includes integration of the ND4-module (17). In summary, we conclude that TMEM126A is an assembly factor for the ND4-module of complex I and functions independently of its paralog TMEM126B.

Discussion

TMEM126A Is Important for Biogenesis of Mitochondrial Complex I through ND4-Module Assembly. The analysis of proteins involved in mitochondrial disease where no clear molecular function is ascribed is critical to improving diagnosis and, potentially, future patient outcomes. Mutations in *TMEM126A* have been identified in numerous cases of AROA (5, 7–9); however, a detailed molecular function of this protein has been lacking. From the reported cases of patients with mutations in TMEM126A that result in optic atrophy, one patient was reported to have a "partial deficiency of complex I" in patient-derived fibroblasts (5). While an MRI conducted was considered normal, the patient was reported to have moderate hypertrophic cardiomyopathy, which is a more common presentation for patients with complex I deficiency (2, 4, 5, 35). Analysis of TMEM126A-interacting proteins revealed an association with TMEM70, a protein long known to play a role in assembly of ATP synthase through incorporation of subunit c into the complex V rotor (36, 37) but more recently also implicated in assembly of the complex I ND4-module (P_D-a intermediate) (17, 32).

Assembly factors have been found to play important roles during the biogenesis of complex I, including the delivery of cofactors (38), posttranslational modification of subunits (39–41), the insertion of subunits into the inner membrane and stabilization of incompletely assembled modules (20). Previous studies have started to elucidate a clearer picture for the assembly of the distal membrane arm of complex I, with a number of assembly factors identified to participate in the biogenesis of this region including FOXRED1, TMEM70, DMAC1, and DMAC2 (16, 17, 42). Indeed, complexome profiling has previously demonstrated that DMAC2, FOXRED1, and TMEM70 comigrate with subunits of the ND4-module of complex I during assembly (17). Surprisingly, TMEM126A was not detected with these complex I assembly intermediates (17). Interestingly, of these ND4-module assembly factors, TMEM126A only enriched TMEM70 and not FOXRED1 or DMAC2, suggesting that while they participate in assembly of the same module, they may not participate during the same stage of this process. Indeed, our analysis demonstrated a strong enrichment of newly synthesized ND4 protein associated with TMEM126A. Also, TMEM126A-containing complexes were strongly disrupted in NDUFB10^{KO} mitochondria—a subunit belonging to the ND4-module whose loss leads to turnover of all ND4-module subunits, including ND4 itself (16, 30). The clinical link between TMEM126A and assembly of the ND4-module is further supported by the numerous patients with the maternally inherited mtDNA m.11778G > A mutation in the *MT-ND4* gene, the most common mtDNA mutation that leads to LHON, which is a similar degenerative condition that affects the optic nerve neurons (43–46). We propose that TMEM126A plays a prominent role in the assembly of complex I through association with the ND4-module, and loss of this protein results in decreased levels of complex I leading to optic atrophy. Future genetic diagnosis of patients with complex I deficiency should consider the possibility of genetic variants in the *TMEM126A* gene as a possible cause of mitochondrial disease.

Duplication and Specialization of the TMEM126 Locus. The ancestral *TMEM126A* gene appeared to undergo a duplication event giving rise to TMEM126A and TMEM126B, both having a role in the assembly of complex I (12). Given the recent duplication at the root of mammalian evolution, these genes have undergone rapid adaptation and associate with distinct membrane assembly intermediates of complex I–TMEM126B as part of the MCIA complex required for ND2-module (14) and here, we show that TMEM126A associates with ND4. Both the ND2 and ND4 subunits are membrane proteins that have evolved from the ancient Na^+/H^+ Mrp antiporter complex (47). This alludes to some interesting questions for nonmammalian metazoans where only TMEM126A is found. Analysis of complex I assembly defects in fly muscle upon knockdown of the subunits *Drosophila* (d)NDUFV1 or dNDUFS5 revealed the presence of a complex I intermediate consisting of the distal portion of the membrane arm of complex I (including the ND4-module), conserved components of the MCIA complex as well as the *Drosophila* homolog of TMEM126A, termed dTMEM126B (48). Might this ancestral protein be involved in assembly of two distinct complex I modules? Interestingly, in addition to TMEM126A and TMEM126B sharing an evolutionary origin, the transmembrane proteins TMEM70 (involved in ND4-module assembly) and TMEM186 (involved in ND2-module assembly by interacting with ND3) also share a common ancestor (14, 17, 32). This may suggest potential symmetry involved in the assembly and integration of the ND2- and ND4-modules. From an evolutionary perspective, further studies could provide useful insights into how complex I assembly has adapted over time. It is also unclear why loss of TMEM126A from mammalian cells is less severe than the loss of TMEM126B with residual complex I assembly and activity observed, given that TMEM126A came first. Indeed, individuals with mutations in TMEM126A primarily present with optic atrophy and most have been identified with homozygous nonsense mutations (5, 6). This is in contrast to individuals with TMEM126B mutations who present with adult-onset myopathy and all identified cases have at least one missense mutation, suggesting total ablation of TMEM126B may not be compatible with human life (22, 23). One possibility is that TMEM126B plays a crucial role in the MCIA complex for ND2-module assembly, while other (unidentified) mitochondrial machineries may be able to compensate for the loss of TMEM126A for ND4-module assembly. Further studies into the role of TMEM126A as a new component of the complex I assembly machinery and its evolutionary relationship with TMEM126B are warranted to uncover the mechanism behind these observations.

Methods and Materials

Cell Culturing. HEK293T cells (American Type Culture Collection; CRL-3216) were cultured in Dulbecco's Modified Eagle's Medium (DMEM) supplemented with 10% (vol/vol) Fetal Bovine Serum (FBS; Life Technologies; 10499-044), 1% penicillin-streptomycin (P/S; Sigma-Aldrich; P3358), 1× GlutaMAX (Life Technologies; 35050061), and 50 μg/mL uridine (Sigma-Aldrich; U6381). For galactose

screening of the TMEM126A/126B^{DKO} cell line, glucose-free DMEM (Life Technologies; 11966-025) was supplemented with 10% (vol/vol) FBS, 25 mM D-(+)-galactose (Sigma-Aldrich; G0750), 1% P/S, 1× GlutaMAX, 1 mM sodium pyruvate (Life Technologies; 11360070), and 50 μg/mL uridine. All cells were incubated at 37 °C with 5% CO_2 in a humidified environment.

For SILAC experiments, cells were cultured as previously described (16). Knockout cell lines and their respective controls were grown in DMEM without lysine and arginine, supplemented with 10% (vol/vol) dialyzed FBS (GE Healthcare; SH30079.03), 1% P/S, 1× GlutaMAX Supplement, 1 mM sodium pyruvate, and 50 μg/mL uridine (Sigma-Aldrich; U6381). Media also contained either "light" lysine and arginine (Lysine; Sigma-Aldrich; L5626, Arginine; Sigma-Aldrich; A5131) or "heavy" $^{13}C_6{}^{15}N_2$-Lysine (Silantes; 211604102) and $^{13}C_6{}^{15}N_4$-Arginine (Cambridge Isotope Labs Inc; CNLM-539-H-1). Cells were cultured in SILAC "light" or "heavy" media for 2 wk prior to harvesting by centrifugation (800 × *g*, 5 min, 4 °C), followed by mitochondrial isolation and quantitative proteomics (described below).

Cloning and Molecular Biology. CRISPR/Cas9 gene editing was performed using the pSpCas9(BB)-2A-GFP (×458) plasmid construct [a gift from F. Zhang; Addgene; plasmid 48138 (49)]. Gene-specific target sites and guide RNAs (gRNAs) were designed using the web-based tool, CHOPCHOP (50). Targeting strategies and gRNA sequences are detailed in *SI Appendix*, Table S1. For the generation of rescue cell lines, complementary DNA (cDNA) from target genes were amplified from a HEK293T cDNA library with a 3′ Flag sequence incorporated into the reverse primer. The constitutively expressed retroviral vector pBABE-puro [Addgene; plasmid 1764 (51)] was used to express the cDNA of interest. Sequence verification of all plasmid constructs was performed by Micromon Genomics (Monash University).

Transfection and Stable Cell Line Generation. Cells were transfected using Lipofectamine LTX and PLUS Reagents (Life Technologies; 15338100) according to the manufacturer's instructions. Stable cell lines expressing the protein of interest were generated by transfecting HEK293T cells with pBABE-puro constructs encoding the desired cDNA. Retroviral supernatants were harvested after 48 h, filtered through a 0.45 μm filter (Merck; SLHV033RS), and used for transduction of knockout cell lines with the addition of 8 μg/mL polybrene. Infected cells were selected for by the addition of 2 μg/mL puromycin (InvivoGen; ant-pr). Expression was verified by SDS-PAGE and/or BN-PAGE analysis.

Gene Editing and Screening. Clonal knockout cell populations were generated by fluorescence-activated cell sorting (FACS) for green fluorescent protein expression (encoded in the CRISPR/Cas9 construct) 24 h post transfection. FACS analysis and single-cell sorting was performed by Flowcore (Monash University). Loss of TMEM126A was screened by PCR of extracted genomic DNA and subsequent Western blotting analysis. Respiratory complex I–deficient TMEM126A/B^{DKO} clones were identified by a growth defect on galactose-based DMEM and subsequent Western blotting analysis. Knockout cell lines were verified by sequence identification of individual indels (*SI Appendix*, Table S1) as previously described (52). Complete loss of a protein product was further validated by SDS-PAGE and/or BN-PAGE. Other complex I accessory subunit and assembly factor KO lines are described elsewhere (*SI Appendix*, Table S1) (14, 16).

Mitochondrial Isolation, Gel Electrophoresis, Immunoblotting, and In-Gel Activity Assay. Mitochondria were isolated from cultured cells by differential centrifugation as previously described (14, 53). Quantitation of protein concentration was estimated by bicinchoninic acid (BCA) assay using the Thermo Scientific Pierce BCA Protein Assay kit (Thermo Fisher Scientific; 23227).

PAGE techniques were performed as previously described (14, 29, 54, 55). For SDS-PAGE, crude mitochondrial samples were solubilized in 2× SDS loading dye (100 mM Tris-Cl pH 6.8, 200 mM dithiothreitol (DTT), 4% (wt/vol) SDS, 20% (vol/vol) glycerol, 0.1% bromophenol blue) or 1× LDS Sample Buffer (Thermo Fisher Scientific; NP0008) supplemented with 100 mM DTT. For Western blotting, 10% acrylamide gels were used while continuous 10 to 16.5% gels were used for separation of radiolabeled proteins. For BN-PAGE analysis of mitochondrial complexes, crude mitochondria were solubilized in 1% digitonin or 1% Triton X-100 in solubilization buffer (20 mM Bis-Tris pH 7.0, 50 mM NaCl, 10% (vol/vol) glycerol) for 10 min on ice, followed by centrifugation at 16,000 × *g* for 10 min. The supernatant was separated from the pellet of unsolubilized material and mixed with 10× BN loading dye (500 mM ε-amino n-caproic acid, 100 mM Bis-Tris pH 7.0, 5% (wt/vol) Coomassie Brilliant Blue G-250) to a final 1× concentration. Western transfer onto Immoiblon-P polyvinylidene difluoride (PVDF) membranes (Merck Millipore; IPVH00010) was performed using the Power Blotter XL System (Thermo Fisher Scientific; PB0013) or Novex Semi-Dry Blotter (Thermo Fisher Scientific; SD1000) in accordance with the manufacturer's instructions. Blots were stained in PVDF stain (50% (vol/vol) methanol, 7% (vol/vol) acetic acid, 0.1% (wt/vol) Coomassie Brilliant Blue R-250), and excess Coomassie was removed by incubating in PVDF destain (50% (vol/vol) methanol, 7% (vol/vol) acetic acid). PVDF stain was completely removed with 100% methanol and blots were subsequently washed in Tris-buffered Saline (TBS; 20 mM Tris-Cl pH 7.5, 150 mM NaCl) with 0.1% Tween-20 (TBS-T). The primary antibodies used in this study are as follows: ACAD9 [in-house; (14)], ATP5A (Abcam; ab14748), Core 1 (Thermo Fisher Scientific; 459140), COX4 (Abcam; ab110261), ECSIT [in-house (14)], Flag (M2 clone; Sigma-Aldrich; F1804), ND4 (Abcam; ab219822), NDUFAF1 [in-house (14)], NDUFB8 (Abcam; ab110242), NDUFB10 (Abcam; ab196019), NDUFC2 (Santa Cruz Biotechnology; sc-398719), SDHA (Abcam; ab14715), TIMMDC1 (Sigma-Aldrich; HPA053214), TMEM126A (Sigma-Aldrich; HPA046648), and TMEM126B (Sigma-Aldrich; HPA014480). Horseradish peroxidase–coupled secondary antibodies (anti-mouse IgG; Sigma-Aldrich; A9044, anti-rabbit-IgG; Sigma-Aldrich; A0545) were used with Clarity Western enhanced chemiluminescence (ECL) substrate (Bio-Rad; 1705061) and Clarity Max Western ECL Substrate (Bio-Rad; 1705062) for detection with the ChemiDocTM XRS+ System (Bio-Rad).

For densitometric analysis, Western blot exposures were analyzed in ImageLab software (Bio-Rad) by drawing a box around the region of interest as well as a separate region for background correction. The same sized box was the used for all samples to be analyzed. Pixel intensity was also measured for a loading control. The normalized signal intensity was then taken as a percentage of control samples and analyzed using GraphPad Prism (version 7.01).

For in-gel activity assay, isolated mitochondria were solubilized in 1% digitonin or 1% TX100 in solubilization buffer, subjected to BN-PAGE, and incubated with 0.1 mg/mL NADH (Sigma-Aldrich; N8129), 2.5 mg/mL nitrotetrazolium blue (Thermo Fisher Scientific; N6495) in 5 mM Tris-HCl pH 7.4 until a violet color developed (56).

Radiolabeling of mtDNA-Encoded Proteins and Affinity Enrichment Analysis. Cells were cultured for radiolabeling as previously described (14, 33). To summarize, cells were labeled in Met/Cys-free DMEM (Life Technologies; 21013024), supplemented with 10% (vol/vol) dialyzed FBS, 1% P/S, 1× GlutaMAX, 1 mM sodium pyruvate, 50 μg/mL uridine, 7 μg/mL anisomycin (Sigma-Aldrich; A9789), and 7 μCi [^{35}S]-Methionine/cysteine (PerkinElmer; NEG072007MC) and labeled for 2 h. Labeling was quenched with 10 μM "cold" methionine (Sigma-Aldrich; M9625) and replaced with standard DMEM growth media for 0, 3, or 24 h. Cells were harvested by centrifugation (800 × *g*, 5 min, 4 °C). Pellets were stored at −20 °C until use. Isolated mitochondria from radiolabeled cells were used for Flag affinity enrichment and SDS-PAGE analysis and immunoblotting. Detection of radiolabeled mt-DNA subunits was performed using an Amersham Typhoon Biomolecular Imager (GE Healthcare).

For affinity enrichment of Flag-tagged proteins, mitochondria were solubilized with 1% digitonin in solubilization buffer (20 mM Bis-Tris pH 7.0, 50 mM NaCl, 10% (vol/vol) glycerol) for 10 min on ice. Solubilized mitochondria were then clarified by centrifugation at 16,000 × *g* for 10 min and incubated with prewashed anti-Flag M2 Affinity Gel (Merck; A2220) at 4 °C for 2 h. Following affinity purification, Flag affinity gel was washed with 0.1% digitonin in solubilization buffer. For samples used for proteomics or Western blotting analysis, Flag-tagged proteins were eluted by incubation with 150 μg/mL Flag tag peptide (Merck; F3290) with 0.1% digitonin in solubilization buffer for 30 min at 4 °C. Eluates were then prepared for SDS-PAGE by the addition of 4× SDS loading dye or for proteomics analysis as described below. For pulse–chase experiments, enriched proteins were removed from the Flag affinity gel by incubating beads in 2× SDS loading dye (100 mM Tris-Cl pH 6.8, 200 mM DTT, 4% (wt/vol) SDS, 20% (vol/vol) glycerol, 0.1% bromophenol blue) at room temperature for 15 min and separated from the affinity gel by centrifugation at 16,000 × *g* for 10 min.

Proteomics Sample Preparation. For SILAC analysis, control and T126A^{KO} cells were cultured in "Heavy" and "Light" SILAC media as described above. Sample preparation was performed as previously described with some modifications (14, 16, 57). Briefly, protein concentrations were determined by BCA and equal amounts of differently labeled control and T126A^{KO} cells were mixed and mitochondria isolated as described. Two samples were heavy-labeled T126A^{KO} cells and light control–labeled cells, while a third consisted of a label switch.

For pulse–chase SILAC, control and T126A^{KO} cells (in triplicate for each timepoint assessed) were cultured overnight in light SILAC DMEM in the presence of 50 μg/mL chloramphenicol. The following day, the light SILAC media was removed, and cells were washed with phosphate-buffered saline

(PBS) prior to the addition of heavy SILAC DMEM. For the SILAC pulse, cells were incubated for the indicated times and the cells were then harvested and frozen at −80 °C. For the chase, SILAC heavy media was removed and cells washed with PBS and replaced with light SILAC media. Note that the "4 h pulse" sample was also used as the "0 h chase" sample. Mitochondria were subsequently isolated and subjected to proteomics sample preparation.

Following mitochondrial isolation for both SILAC experiments, samples were solubilized in 1% (wt/vol) sodium deoxycholate, 100 mM Tris-Cl pH 8.1, 40 mM chloroacetamide, and 10 mM Tris(2-carboxyethyl)phosphine hydrochloride (TCEP) prior to vortexing and heating for 5 min at 99 °C with vigorous shaking at 1,400 rpm. Samples were then sonicated in a water bath at room temperature for 15 min. Proteomic digestion was performed by the addition of 1 μg proteomics-grade Trypsin (Promega; V5113) to 100 μg protein and incubated overnight at 37 °C. Supernatants were mixed with ethyl acetate (99%(vol/vol)) and trifluoroacetic acid (TFA) (1% (vol/vol)), then transferred to 3× 14G 3M Empore styrenedivinylbenzene-reverse phase sulfonate stage tips (58). Samples were then centrifuged through the stage tip at 3,000 × *g* at room temperature (58). Stage tips were then washed with 99% (vol/vol) ethyl acetate with 1% (vol/vol) TFA, followed by a second wash with 99% (vol/vol) ethyl acetate and 0.2% (vol/vol) TFA. Samples were eluted with 80% (vol/vol) acetonitrile (ACN) and 1% (vol/vol) NH_4OH and acidified to a final TFA concentration 1% (vol/vol) before drying samples down in a SpeedVac.

For affinity enrichment sample preparation, elutions were precipitated using five volumes of ice-cold acetone and incubated at −20 °C overnight. Samples were centrifuged at 16,000 × *g* for 10 min at 4 °C, following which the precipitated pellet was solubilized in 8 M urea and 50 mM ammonium bicarbonate. This was sonicated in a water bath at room temperature for 15 min before addition of 5 mM TCEP and 50 mM chloroacetamide (Sigma-Aldrich) and incubated at 37 °C while shaking. The sample was then treated with ammonium bicarbonate to dilute the urea to a final concentration of 2 M. Sequencing grade modified trypsin (1 μg; Promega; V5113) was added to the sample (eluate from 500 μg mitochondrial protein) before incubation overnight at 37 °C. After this the sample was acidified with 10% (vol/vol) TFA to a final concentration of 1% (vol/vol). Stage tips were generated with two plugs of 3 M Empore Styrenedivinylbenzene-Copolymer Extraction Disks (Fisher Scientific) that were activated with 100% (vol/vol) ACN via centrifugation. All spins were performed at 1,800 *g*. The tips were washed with 0.1% (vol/vol) TFA and 2% (vol/vol) ACN three times. The sample was added to the stage tip and eluted with 80% (vol/vol) ACN and 0.1% (vol/vol) TFA. The eluates were subsequently dried down using a SpeedVac.

SILAC and AE-MS Proteomics Analysis. Peptides were reconstituted in 2% (vol/vol) ACN and 0.1% (vol/vol) TFA and transferred to autosampler vials for analysis by online nano-high-performance liquid chromatography (HPLC)/electrospray ionization-MS/MS using a Thermo Scientific Orbitrap QE plus (SILAC) and Elite (AE-MS) instrument connected to an Ultimate 3000 HPLC. Instrument parameters and HPLC build and chromatography settings were described in detail in ref. 14.

For the SILAC and AE-MS experiments, raw files were analyzed using the MaxQuant platform (59) version 1.6.5.0 searching against the UniProt human database containing reviewed, canonical entries (January 2019) and a database containing common contaminants. Parameters used in the SILAC and LFQ searches are described in Formosa et al. (14). Statistical analysis was performed using the Perseus platform (60) version 1.6.7.0. Briefly, for the SILAC experiment, the label switch sample was inverted and the resultant heavy/light ratio values were $\log_2$-transformed. Proteins present in the Mitocarta2.0 database (61) were matched according to gene name. Samples with ratios for <2 of 3 replicates were removed from the analysis and a single-sample two-sided Student's *t* test performed. Nonmitochondrial (defined as not present in Mitocarta2.0) were removed prior to further analysis. For topographical heatmapping, $\log_2$-transformed median SILAC ratios were mapped onto homologous subunits of the respiratory chain complexes as described in Formosa, et al. (14). To define significant changes in the TMEM126A^{KO} mitochondrial proteome, we used a threshold of fold change value 1.5 ($\log2 \pm 0.585$) and a *P* value of <0.05. For the AE-MS experiment, LFQ Intensities were $\log_2$ transformed and the replicates assigned to TMEM126A^{Flag} or control experimental groups. Rows were filtered such that at least one replicate in the TMEM126A^{Flag} group was valid. Missing values in the control group were imputed to simulate the limit of detection based on the distribution of all values detected in the samples (downshift of 1.8, width 0.3). To determine the significance of proteins enriched in the TMEM126A^{Flag}, a two-sided, two-sample *t* test between groups was performed, with significance ascertained through permutation-based false discovery rate (FDR) statistics (FDR 5%, s0 = 1.5). This test incorporates the modified test statistic approach described by Tusher et al. (62) where s0 controls the relative importance of the resulted *P* value and difference between the means of the two sample groups. For this experiment, the s0 parameter was determined by iteratively increasing the parameter until all identifications enriched in the control samples were excluded from significance.

Pulse–Chase SILAC Proteomics. For the pulse–chase SILAC experiment, analysis was performed on a Thermo Scientific Orbitrap Eclipse instrument connected to an Ultimate 3000 HPLC. The HPLC build is described in detail in ref. 14, but the chromatography is summarized below. Tryptic peptides were injected to the trap column at an isocratic flow of 6 μL/min of 2% (vol/vol) ACN containing 0.1% (vol/vol) formic acid for 5 min applied before the trap column was switched in line with the analytical column. The eluents were 5% dimethyl sulfoxide (DMSO) in 0.1% (vol/vol) formic acid (solvent A) and 5% DMSO in 100% (vol/vol) ACN and 0.1% (vol/vol) formic acid (solvent B). The flow gradient was 1) 0 to 6 min at 3% B, 2) 6 to 95 min, 3 to 23% B, 3) 95 to 105 min 23 to 40% B, 4) 105 to 110 min, 40 to 80% B, 5) 110 to 115 min, 80 to 80% B, and 6) 115 to 117 min, 80 to 3% and equilibrated at 3% B for 10 min before the next sample injection. The Orbitrap Eclipse mass spectrometer was operated in the data-dependent mode with a targeted inclusion list containing predicted peptides from the 13 mtDNA-encoded proteins as previously described (34). Acquisition method was created with the Orbitrap Tribrid Tune version 3.3 acquisition software. The Full MS1 spectra from 375 to 1,500 m/z was acquired in positive mode at 120,000 resolution. Two scan priorities were created post MS1 scans. The first priority was given to precursors that fulfill the mass and charge criteria. Precursors were then isolated using an isolation window of 1.6 *m/z* and precursors fragmented using fixed normalized collision energy of 30. MS2 resolution was at 15,000, automatic gain control target at 5^5 and maximum injection time (IT) time of 100 ms. The second scan priority is activated when no matching mass from the targeted list. Precursors were isolated with the same parameters with the difference of maximum IT time of 22 ms. Dynamic exclusion was set to 30 s.

Raw files were processed using the MaxQuant platform (version 1.6.10.43) (59) and searched against the UniProt human database (November 2019) using default settings for a SILAC experiment with "multiplicity" set to "2" and "Heavy labels" selected to "Arg10" and "Lys8," "label min. ratio count" set to 1 and match between runs and requantify enabled. From the proteinGroups.txt output file, mtDNA-encoded proteins were filtered by gene name, and protein entries identified by a single peptide and samples containing less than 70% valid values were removed prior to data analysis using the Perseus software package (version 1.6.10.43) (60). Heavy intensities were $\log_2$ transformed and normalized to the maximum value detected in the wild-type cell line at 4 h pulse. The means were plotted over time using Prism along with the SD in Prism (version 8.4.3, GraphPad). Statistical significance was performed in Prism using *t* test with the two-stage step-up method of Benjamini, Krieger, and Yekutieli and FDR of 5%.

Data Availability. The mass spectrometry proteomics data have been deposited in the ProteomeXchange Consortium via the PRIDE (63) partner repository (https://www.ebi.ac.uk/pride/archive) with the dataset identifier PXD023136 (64).

ACKNOWLEDGMENTS. We thank the Bio21 Mass Spectrometry and Proteomics Facility and the Monash Proteomics and Metabolomics Facility for the provision of instrumentation, training, and technical support and Monash Flowcore for cell sorting. We acknowledge funding from the National Health and Medical Research Council (NHMRC Project Grants 1164459 and 1165217 to M.T.R.; 1125390 to M.T.R. and D.A.S.; NHMRC Fellowship 1140851 to D.A.S.).

1. J. B. Spinelli, M. C. Haigis, The multifaceted contributions of mitochondria to cellular metabolism. *Nat. Cell Biol.* **20**, 745–754 (2018).
2. A. E. Frazier, D. R. Thorburn, A. G. Compton, Mitochondrial energy generation disorders: Genes, mechanisms, and clues to pathology. *J. Biol. Chem.* **294**, 5386–5395 (2019).
3. A. Signes, E. Fernandez-Vizarra, Assembly of mammalian oxidative phosphorylation complexes I-V and supercomplexes. *Essays Biochem.* **62**, 255–270 (2018).
4. G. S. Gorman *et al.*, Mitochondrial diseases. *Nat. Rev. Dis. Primers* **2**, 16080 (2016).
5. S. Hanein *et al.*, TMEM126A, encoding a mitochondrial protein, is mutated in autosomal-recessive nonsyndromic optic atrophy. *Am. J. Hum. Genet.* **84**, 493–498 (2009).
6. E. Meyer *et al.*, Nonsense mutation in TMEM126A causing autosomal recessive optic atrophy and auditory neuropathy. *Mol. Vis.* **16**, 650–664 (2010).

7. J. Désir *et al*., TMEM126A mutation in a Moroccan family with autosomal recessive optic atrophy. *Mol. Vis.* **18**, 1849–1857 (2012).
8. K. Kloth *et al*., Novel likely pathogenic variants in TMEM126A identified in non-syndromic autosomal recessive optic atrophy: Two case reports. *BMC Med. Genet.* **20**, 62 (2019).
9. C. La Morgia *et al*., First *TMEM126A* missense mutation in an Italian proband with optic atrophy and deafness. *Neurol. Genet.* **5**, e329 (2019).
10. V. Carelli *et al*., Retinal ganglion cell neurodegeneration in mitochondrial inherited disorders. *Biochim. Biophys. Acta* **1787**, 518–528 (2009).
11. S. Hanein *et al*., TMEM126A is a mitochondrial located mRNA (MLR) protein of the mitochondrial inner membrane. *Biochim. Biophys. Acta* **1830**, 3719–3733 (2013).
12. D. M. Elurbe, M. A. Huynen, The origin of the supernumerary subunits and assembly factors of complex I: A treasure trove of pathway evolution. *Biochim. Biophys. Acta* **1857**, 971–979 (2016).
13. H. Heide *et al*., Complexome profiling identifies TMEM126B as a component of the mitochondrial complex I assembly complex. *Cell Metab.* **16**, 538–549 (2012).
14. L. E. Formosa *et al*., Dissecting the roles of mitochondrial complex I intermediate assembly complex factors in the biogenesis of complex I. *Cell Rep.* **31**, 107541 (2020).
15. B. Andrews, J. Carroll, S. Ding, I. M. Fearnley, J. E. Walker, Assembly factors for the membrane arm of human complex I. *Proc. Natl. Acad. Sci. U.S.A.* **110**, 18934–18939 (2013).
16. D. A. Stroud *et al*., Accessory subunits are integral for assembly and function of human mitochondrial complex I. *Nature* **538**, 123–126 (2016).
17. S. Guerrero-Castillo *et al*., The assembly pathway of mitochondrial respiratory chain complex I. *Cell Metab.* **25**, 128–139 (2017).
18. M. Lazarou, M. McKenzie, A. Ohtake, D. R. Thorburn, M. T. Ryan, Analysis of the assembly profiles for mitochondrial- and nuclear-DNA-encoded subunits into complex I. *Mol. Cell. Biol.* **27**, 4228–4237 (2007).
19. C. Ugalde *et al*., Human mitochondrial complex I assembles through the combination of evolutionary conserved modules: A framework to interpret complex I deficiencies. *Hum. Mol. Genet.* **13**, 2461–2472 (2004).
20. L. E. Formosa, M. G. Dibley, D. A. Stroud, M. T. Ryan, Building a complex complex: Assembly of mitochondrial respiratory chain complex I. *Semin. Cell Dev. Biol.* **76**, 154–162 (2018).
21. L. Sánchez-Caballero, S. Guerrero-Castillo, L. Nijtmans, Unraveling the complexity of mitochondrial complex I assembly: A dynamic process. *Biochim. Biophys. Acta* **1857**, 980–990 (2016).
22. L. Sánchez-Caballero *et al*., Mutations in complex I assembly factor TMEM126B result in muscle weakness and isolated complex I deficiency. *Am. J. Hum. Genet.* **99**, 208–216 (2016).
23. C. L. Alston *et al*., Biallelic mutations in TMEM126B cause severe complex I deficiency with a variable clinical phenotype. *Am. J. Hum. Genet.* **99**, 217–227 (2016).
24. K. Thompson *et al*., *OXA1L* mutations cause mitochondrial encephalopathy and a combined oxidative phosphorylation defect. *EMBO Mol. Med.* **10**, e9060 (2018).
25. Y. H. Lin, N. K. Wang, L. Yeung, C. C. Lai, L. H. Chuang, Juvenile open-angle Glaucoma associated with Leber's hereditary optic neuropathy: A case report and literature review. *BMC Ophthalmol.* **18**, 323 (2018).
26. D. D. De Vries *et al*., Genetic and biochemical impairment of mitochondrial complex I activity in a family with Leber hereditary optic neuropathy and hereditary spastic dystonia. *Am. J. Hum. Genet.* **58**, 703–711 (1996).
27. J. Gu *et al*., The architecture of the mammalian respirasome. *Nature* **537**, 639–643 (2016).
28. U. Schlattner, M. Tokarska-Schlattner, T. Wallimann, Mitochondrial creatine kinase in human health and disease. *Biochim. Biophys. Acta* **1762**, 164–180 (2006).
29. M. McKenzie, M. Lazarou, D. R. Thorburn, M. T. Ryan, Analysis of mitochondrial subunit assembly into respiratory chain complexes using Blue Native polyacrylamide gel electrophoresis. *Anal. Biochem.* **364**, 128–137 (2007).
30. K. Fiedorczuk *et al*., Atomic structure of the entire mammalian mitochondrial complex I. *Nature* **538**, 406–410 (2016).
31. J. Zhu, K. R. Vinothkumar, J. Hirst, Structure of mammalian respiratory complex I. *Nature* **536**, 354–358 (2016).
32. L. Sánchez-Caballero *et al*., TMEM70 functions in the assembly of complexes I and V. *Biochim. Biophys. Acta Bioenerg.* **1861**, 148202 (2020).
33. L. E. Formosa, A. Hofer, C. Tischner, T. Wenz, M. T. Ryan, Translation and assembly of radiolabeled mitochondrial DNA-encoded protein subunits from cultured cells and isolated mitochondria. *Methods Mol. Biol.* **1351**, 115–129 (2016).
34. D. H. Hock *et al*., HIGD2A is required for the assembly of the COX3 module of human mitochondrial complex IV. *Mol. Cell. Proteomics* **19**, 1145–1160 (2020).
35. A. E. Frazier *et al*., Fatal perinatal mitochondrial cardiac failure caused by recurrent De Novo duplications in the ATAD3 locus. *Med (N. Y.)* **2**, 49–73 (2020).
36. J. Kovalčíková *et al*., TMEM70 facilitates biogenesis of mammalian ATP synthase by promoting subunit c incorporation into the rotor structure of the enzyme. *FASEB J.* **33**, 14103–14117 (2019).
37. R. Spiegel *et al*., TMEM70 mutations are a common cause of nuclear encoded ATP synthase assembly defect: Further delineation of a new syndrome. *J. Med. Genet.* **48**, 177–182 (2011).
38. A. D. Sheftel *et al*., Human ind1, an iron-sulfur cluster assembly factor for respiratory complex I. *Mol. Cell. Biol.* **29**, 6059–6073 (2009).
39. V. F. Rhein, J. Carroll, S. Ding, I. M. Fearnley, J. E. Walker, NDUFAF5 hydroxylates NDUFS7 at an early stage in the assembly of human complex I. *J. Biol. Chem.* **291**, 14851–14860 (2016).
40. V. F. Rhein, J. Carroll, S. Ding, I. M. Fearnley, J. E. Walker, NDUFAF7 methylates arginine 85 in the NDUFS2 subunit of human complex I. *J. Biol. Chem.* **288**, 33016–33026 (2013).
41. O. Zurita Rendón, L. Silva Neiva, F. Sasarman, E. A. Shoubridge, The arginine methyltransferase NDUFAF7 is essential for complex I assembly and early vertebrate embryogenesis. *Hum. Mol. Genet.* **23**, 5159–5170 (2014).
42. L. E. Formosa *et al*., Characterization of mitochondrial FOXRED1 in the assembly of respiratory chain complex I. *Hum. Mol. Genet.* **24**, 2952–2965 (2015).
43. M. D. Brown, J. C. Allen, G. P. Van Stavern, N. J. Newman, D. C. Wallace, Clinical, genetic, and biochemical characterization of a Leber hereditary optic neuropathy family containing both the 11778 and 14484 primary mutations. *Am. J. Med. Genet.* **104**, 331–338 (2001).
44. C. B. Catarino *et al*., Characterization of a Leber's hereditary optic neuropathy (LHON) family harboring two primary LHON mutations m.11778G>A and m.14484T>C of the mitochondrial DNA. *Mitochondrion* **36**, 15–20 (2017).
45. D. C. Wallace *et al*., Mitochondrial DNA mutation associated with Leber's hereditary optic neuropathy. *Science* **242**, 1427–1430 (1988).
46. N. J. Newman, Hereditary optic neuropathies: From the mitochondria to the optic nerve. *Am. J. Ophthalmol.* **140**, 517–523 (2005).
47. L. A. Sazanov, A giant molecular proton pump: Structure and mechanism of respiratory complex I. *Nat. Rev. Mol. Cell Biol.* **16**, 375–388 (2015).
48. C. J. Garcia, J. Khajeh, E. Coulanges, E. I. Chen, E. Owusu-Ansah, Regulation of mitochondrial complex I biogenesis in Drosophila flight muscles. *Cell Rep.* **20**, 264–278 (2017).
49. F. A. Ran *et al*., Genome engineering using the CRISPR-Cas9 system. *Nat. Protoc.* **8**, 2281–2308 (2013).
50. T. G. Montague, J. M. Cruz, J. A. Gagnon, G. M. Church, E. Valen, CHOPCHOP: A CRISPR/Cas9 and TALEN web tool for genome editing. *Nucleic Acids Res.* **42**, W401–W407 (2014).
51. J. P. Morgenstern, H. Land, Advanced mammalian gene transfer: High titre retroviral vectors with multiple drug selection markers and a complementary helper-free packaging cell line. *Nucleic Acids Res.* **18**, 3587–3596 (1990).
52. D. A. Stroud, L. E. Formosa, X. W. Wijeyeratne, T. N. Nguyen, M. T. Ryan, Gene knockout using transcription activator-like effector nucleases (TALENs) reveals that human NDUFA9 protein is essential for stabilizing the junction between membrane and matrix arms of complex I. *J. Biol. Chem.* **288**, 1685–1690 (2013).
53. A. J. Johnston *et al*., Insertion and assembly of human tom7 into the preprotein translocase complex of the outer mitochondrial membrane. *J. Biol. Chem.* **277**, 42197–42204 (2002).
54. I. Wittig, H.-P. P. Braun, H. Schägger, Blue native PAGE. *Nat. Protoc.* **1**, 418–428 (2006).
55. H. Schägger, G. von Jagow, Tricine-sodium dodecyl sulfate-polyacrylamide gel electrophoresis for the separation of proteins in the range from 1 to 100 kDa. *Anal. Biochem.* **166**, 368–379 (1987).
56. E. Zerbetto, L. Vergani, F. Dabbeni-Sala, Quantification of muscle mitochondrial oxidative phosphorylation enzymes via histochemical staining of blue native polyacrylamide gels. *Electrophoresis* **18**, 2059–2064 (1997).
57. M. G. Dibley *et al*., The mitochondrial acyl-carrier protein interaction network highlights important roles for LYRM family members in complex I and mitoribosome assembly. *Mol. Cell. Proteomics* **19**, 65–77 (2020).
58. N. A. Kulak, G. Pichler, I. Paron, N. Nagaraj, M. Mann, Minimal, encapsulated proteomic-sample processing applied to copy-number estimation in eukaryotic cells. *Nat. Methods* **11**, 319–324 (2014).
59. S. Tyanova, T. Temu, J. Cox, The MaxQuant computational platform for mass spectrometry-based shotgun proteomics. *Nat. Protoc.* **11**, 2301–2319 (2016).
60. S. Tyanova *et al*., The Perseus computational platform for comprehensive analysis of (prote)omics data. *Nat. Methods* **13**, 731–740 (2016).
61. S. E. Calvo, K. R. Clauser, V. K. Mootha, MitoCarta2.0: An updated inventory of mammalian mitochondrial proteins. *Nucleic Acids Res.* **44**, D1251–D1257 (2016).
62. V. G. Tusher, R. Tibshirani, G. Chu, Significance analysis of microarrays applied to the ionizing radiation response. *Proc. Natl. Acad. Sci. U.S.A.* **98**, 5116–5121 (2001).
63. Y. Perez-Riverol *et al*., The PRIDE database and related tools and resources in 2019: Improving support for quantification data. *Nucleic Acids Res.* **47**, D442–D450 (2019).
64. L. E. Formosa *et al*., Data from "Optic atrophy-associated TMEM126A is an assembly factor for the ND4-module of mitochondrial complex I." PRIDE. https://www.ebi.ac.uk/pride/archive/projects/PXD023136. Deposited 15 December 2020.
65. L. J. Yan, S. H. Yang, H. Shu, L. Prokai, M. J. Forster, Histochemical staining and quantification of dihydrolipoamide dehydrogenase diaphorase activity using blue native PAGE. *Electrophoresis* **28**, 1036–1045 (2007).